Int J Clin Exp Med 2016;9(7):13372-13383
www.ijcem.com /ISSN:1940-5901/IJCEM0028967

Original Article

Stress distribution over lumbosacral vertebrae and axial transsacral rod after axial lumbar interbody fusion (AxiaLIF): finite element analysis

Lei He[1*], Meichao Zhang[2*], Feng Feng[1], Mao Pang[1], Peigen Xie[1], Ruiqiang Chen[1], Limin Rong[1]

[1]*Department of Spine Surgery, Third Affiliated Hospital, Sun Yat-sen University, Tianhe District, Guangzhou, China;* [2]*Institute of Clinical Anatomy, Southern Medical University, Baiyun District, Guangzhou, China.* [*]*Equal contributors.*

Received March 23, 2016; Accepted June 12, 2016; Epub July 15, 2016; Published July 30, 2016

Abstract: Objective: To evaluate stress distribution over lumbosacral vertebrae and axial transsacral rod by means of finite element analysis. Methods: The intact finite element model was established along L4-S1 lumbosacral vertebrae and validated. To build the standalone AxiaLIF model, an axial transsacral rod was inserted into L5-S1 segment of the validated intact model in accordance with the AxiaLIF technique. For patients with spondylolysis or unilateral direct decompression who received AxiaLIF, corresponding models were established. Comparison of Von Mises stress was made to evaluate the stress distribution endured by bony components or transsacral rod with preload imposed on the models. Results: A higher concentration of stress was registered at the bone-rod interface. The stress distribution over vertebrae was witnessed in the anterior and anterolateral region of S1 vertebra during flexion and axial rotation, while such stress concentration moved to the posterior and lateral region of L5 vertebra in extension and lateral bending respectively. The highest stress turned out to be localizing somewhere one or two thread pitches away from the middle part of the rod. There was no obvious differences of stress distribution among the surgery-simulated models. Conclusion: Standalone AxiaLIF meets the basic need to provide ample stress resistance for body's normal activities. For patients suffering from spondylolysis, or demanding unilateral direct decompression, of no significance was the influence that was exerted on load transfer after AxiaLIF.

Keywords: Lumbosacral vertebrae, transsacral rod, axial lumbar interbody fusion, finite element analysis, stress

Introduction

Lumbosacral degenerative diseases are common causes of chronic low back pain, which usually affect L5-S1 or L4-L5. Accordingly, interbody fusion has emerged as a regular treatment for decades [1, 2].

Lately, axial lumbar interbody fusion (AxiaLIF) has gained widespread attention as a novel percutaneous minimally invasive technique via the axial presacral approach. The procedure eliminates neurovascular retraction and paravertebral structures destruction with the preservation of annulus and ligaments [1]. Due to the unique design of axial transsacral rod, intervertebral space distraction can be achieved associated with favorable axial fixation and bony fusion [1, 2]. It has been revealed by relevant biomechanical tests that AxiaLIF is able to reduce the range of motion, provide significant construct stiffness at the surgical segment and in particular, increase lateral and sagittal bending stiffness [3, 4].

AxiaLIF is a good alternative to traditional lumbar interbody fusion for the treatment of degenerative disc disease or lumbosacral instability such as spondylolysis or low-grade spondylolisthesis at L5-S1 segment [5, 6]. Although clinical outcomes and biomechanical studies have indicated that AxiaLIF offers favorable and durable outcomes associated with sufficient stability [5, 7], the influences on postoperative load transfer and stability of standalone transsacral rod remain elusive. Up until now, there has been no report on the stress distribution over lumbosacral vertebrae and axial transsacral rod in patients with lumbosacral instability who have received standalone AxiaLIF. AxiaLIF is not

Table 1. Material properties used in the finite element models

Materials	Young's Modulus (MPa)	Poisson's ratio	Cross-sec. area (mm^2)
Cortical bone	12000	0.3	
Cancellous bone	100	0.2	
Bony endplates	12000	0.3	
Posterior bony component	3500	0.25	
Cartilage	10	0.4	
Ground substance	4	0.49	
Anulus fiber			
Lateral	106	0.3	6.7
Posterolateral	70.5	0.3	5.8
Anterior	106	0.3	5.5
Posterior	70.5	0.3	3.9
Nucleus pulposus	1	0.499	
Ligaments			
ALL	7.8	0.3	22.4
PLL	10	0.3	7
LF	17	0.3	14.1
ISL	10	0.3	14.1
SSL	8	0.3	10.5
Axial transsacral rod	110000	0.3	

ALL: anterior longitudinal ligament, PLL: posterior longitudinal ligament, LF: ligamentum flavum, ISL: interspinous ligament, SSL: supraspinous ligament.

supposed to be applied in the situation that demands resection of significant portions of the lamina or facets to correct spinal stenosis [8]. As a result, such surgical procedures as micro endoscopic decompressive laminotomy (MEDL) technique, is mandated for posterior direct decompression in an effort to relieve symptoms caused by spinal stenosis [9]. However, the possibility of iatrogenic lumbosacral instability is likely to take place owing to destruction of posterior column. Therefore, evaluation of iatrogenic lumbosacral stability/instability is necessary for patients with unilateral facet deficit resulting from direct decompression in combination with AxiaLIF procedure.

Finite element-based stress analysis has been used progressively in spine biomechanical studies to evaluate internal stress responses of surgical alterations [10]. The objective of this study was to comparatively analyze distribution and magnitude of stresses endured by spinal components and standalone axial transsacral rod in patients with intact lumbosacral vertebrae, spondylolysis or unilateral facet deficit after AxiaLIF procedure using finite element analysis (FEA).

Material and methods

Establishment and validation of the intact model

The three-dimensional nonlinear finite element (FE) model was established over the lumbosacral vertebrae. In such a course, scans of an L4-S1 motion segment were obtained from a healthy male volunteer (age 30, height 176 cm, weight 65 kg), utilizing 320-slice Computed Tomography (CT) (Aquilion One, Toshiba, Tochigi Pref., Japan). The participant gave his written informed consent to the collection and utilization of CT-scan images in the study. The ethical committee of the Third Affiliated Hospital of Sun Yat-sen University has approved this consent procedure and the present study. Sections as thin as 1 mm were automatically reconstructed by MIMICS 14.0 (Materialise Inc., Leuven, Belgium) in line with gray scale. The reconstructed bony components and intervertebral discs were transferred into Freeform v6.0 (SensAble Technologies Inc., Wilmington, MA) to rapidly clean up, modify and stylize scan data. After smoothing the uneven surface caused by the stacking of the medical images, the geometrical model was exported in IGES format. ANSYS 14.0 (ANSYS Inc., Canonsburg, USA) was then used to build the FE model.

The intact FE model was comprised of three vertebrae (L4, L5 and S1), two intervertebral discs (L4-L5 and L5-S1) and major ligaments of the lumbosacral vertebrae. Three-dimensional tetrahedral element was used for the cancellous bone, posterior complex of the vertebrae and axial transascral rod, while cortical bone and vertebral endplates sharing the same node with cancellous elements were modeled as triangular shell element that were 0.5-1.5 mm thick based on the actual anatomic structure [11-13]. Operations were carried out to polish the surfaces of sacral foramen, sacral crest and sacral canal in an effort to simplify the model. Intervertebral discs consisting of disc annulus and disc nucleus were built with hexahedral element [14]. The annulus fibers simulated by nonlinear truss element were

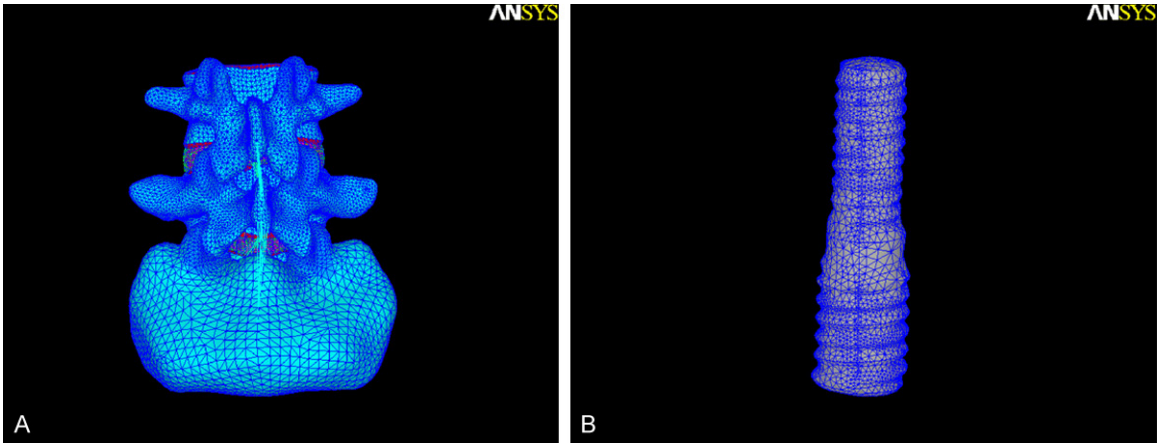

Figure 1. The FE models of intact lumbosacral vertebrae and axial transsacral rod. A. Posterior view of the intact model of L4-S1. B. Anterior view of axial transsacral rod.

assembled alternately at 30° in a radial fashion, which embedded in the ground substance [13]. Materials with incompressible and fluid-like properties were used to generate the nucleus pulposus [12]. The five major ligaments, including anterior longitudinal ligament, posterior longitudinal ligament, ligamentum flavum, interspinous ligament and supraspinous ligament, were modeled by 2-node nonlinear truss element that were subject to tension only. The attached points and cross sectional area of these ligaments were incorporated into relevant nodes of the FE model according to the literature [15]. With a thin cartilaginous layer and a 0.5 mm gap between the articular surfaces, the facet joints were modified as the surface-to-surface interaction. They were assumed to transmit compressive forces only and no friction was supposed between them, either [12, 16]. Material properties of the different tissues obtained from the literatures could be referred to as shown in **Table 1** [11-13, 17].

The intact model of the lumbosacral vertebrae consisted of 395,077 elements and 77,381 nodes (**Figure 1A**). When fixation of inferior surface of the S1 vertebra was firmly secured with all degrees of freedom constrained, an axial compressive preload of 100 N with 10 Nm moment was loaded on the superior surface of L4 vertebra to achieve flexion, extension, lateral bending and axial rotation [18-20].

To validate the intact FE model, intersegmental motions between L4-L5 and L5-S1 were analyzed by ANSYS 14.0 and comparison was also made among the results achieved in previous studies available.

Establishment of surgery-simulated models

In accordance with the actual size of the rod (proximal diameter 14 mm, distal diameter 11 mm, proximal pitch 2.54 mm, distal pitch 2.31 mm, length 45 mm) performed in the AxiaLIF procedure, three-dimensional model of axial transsacral rod (TranS1 Inc, Wilmington, NC) built by Pro/ENGINEER Wildfire 4.0 (PTC Inc., Needham, USA) was imported into ANSYS 14.0 in IGES format (**Figure 1B**). The insertion of the rod into L5-S1 segment of the intact validated model was performed via the presacral approach, followed by the partial volumetric discectomy. Based upon the AxiaLIF technique, the procedure was simulated as radial removal of the nucleus of the L5-S1 segment, while maintaining outer annular integrity [2]. The bone-rod interfaces were assumed to be fully bonded via the node sharing condition to simulate intimate bone-rod purchase [21]. The standalone AxiaLIF model included 386,210 elements and 76,661 nodes shown in **Figure 2A**.

The spondylolysis model without anterior spondylolisthesis included 384,730 elements and 76,700 nodes (**Figure 2B**). In order to simulate bilateral isthmus defects, removal of elements that correspond with pars interarticularis of L5 vertebra was performed in the AxiaLIF model mentioned above. The gaps between bilateral isthmus were set up to avoid any contact [22].

The FE models of unilateral facet deficit including the cases who received either left hemifacetectomy or left facetectomy were also established in line with AxiaLIF model. It actually

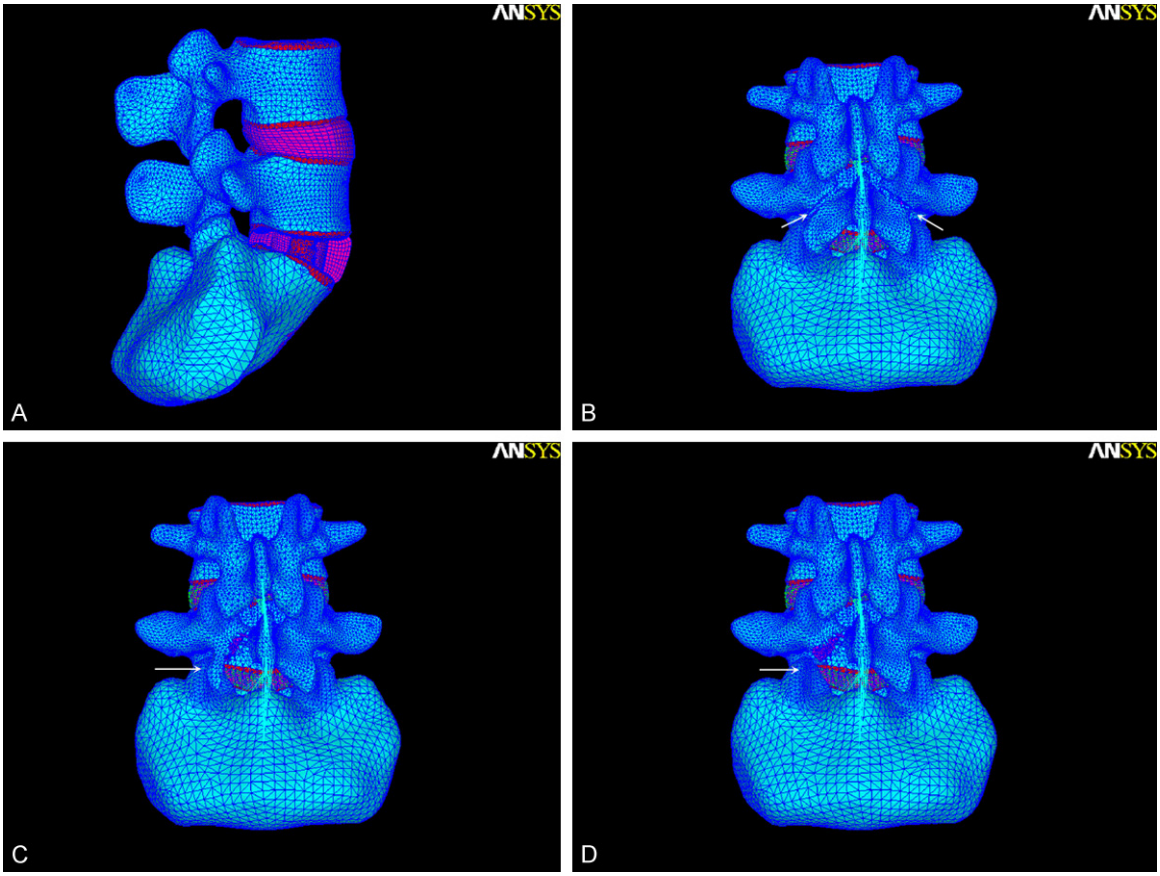

Figure 2. The surgery-simulated FE models. A. Lateral view of AL. B. Posterior view of AL+SP. The arrow illustrated the gaps between bilateral isthmus. C, D. Posterior view of AL+HF and AL+FA. The arrows showed the extent of decompression. AL: standalone AxiaLIF model, AL+SP: spondylolysis model with standalone AxiaLIF procedure, AL+HF: left hemifacetectomy model with standalone AxiaLIF procedure, AL+FA: left facetectomy model with standalone AxiaLIF procedure.

mimicked the anatomic changes for spinal stenosis that was corrected through unilateral decompression at L5-S1 segment by means of MEDL in combination with standalone AxiaLIF. The parts that were resected in left hemifacetectomy model were the medial 1/2 of the left inferior articular process of L5 vertebra and 2/3 inferior aspect of the left lamina of L5 vertebra, in addition to the removal of ligamentum flavum [9, 23]. Left facetectomy model was built on the basis of left hemifacetectomy model. Except resecting all the left inferior articular process of L5 vertebra, other components removal was the same as it in left hemifacetectomy model [9, 23]. These two models were established by 386,211 elements, 75,939 nodes and 383,143 elements, 75,384 nodes, respectively (**Figure 2C**, **2D**).

As assumed to be isotropic and homogenous, the properties of material used in all surgery-simulated models were the same as them in the intact model (**Table 1**). The same boundary and loading conditions were applied to the surgery-simulated models.

Stress analyses

Von Mises stress was compared among the surgery-simulated models for postoperative evaluation of stress distribution and magnitude on spinal components or axial transsacral rod. Furthermore, the probability of internal fixation fracture could be predicted according to the maximum Von Mises stress on the axial transsacral rod, which resulted from an assumption that high stress concentration was likely to induce fixation device failure in the long term.

Results

Validation of intact FE model

A comparison of intersegmental motions in the intact model was made between the results of

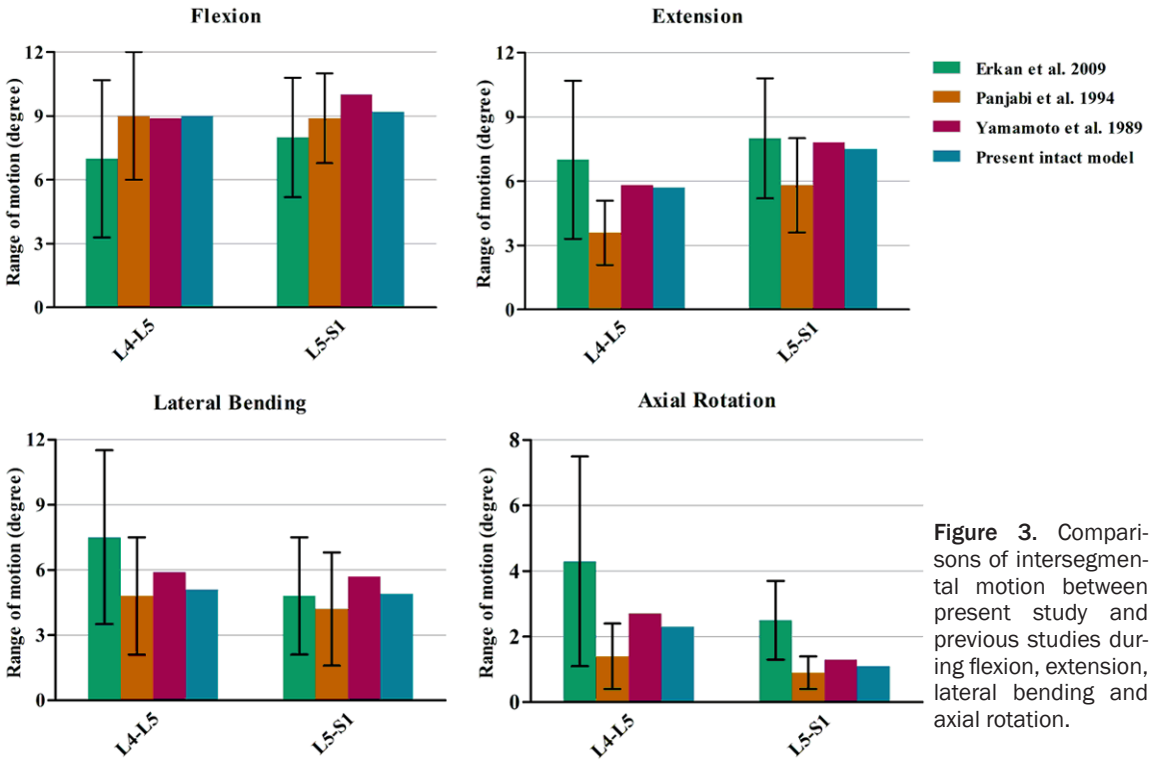

Figure 3. Comparisons of intersegmental motion between present study and previous studies during flexion, extension, lateral bending and axial rotation.

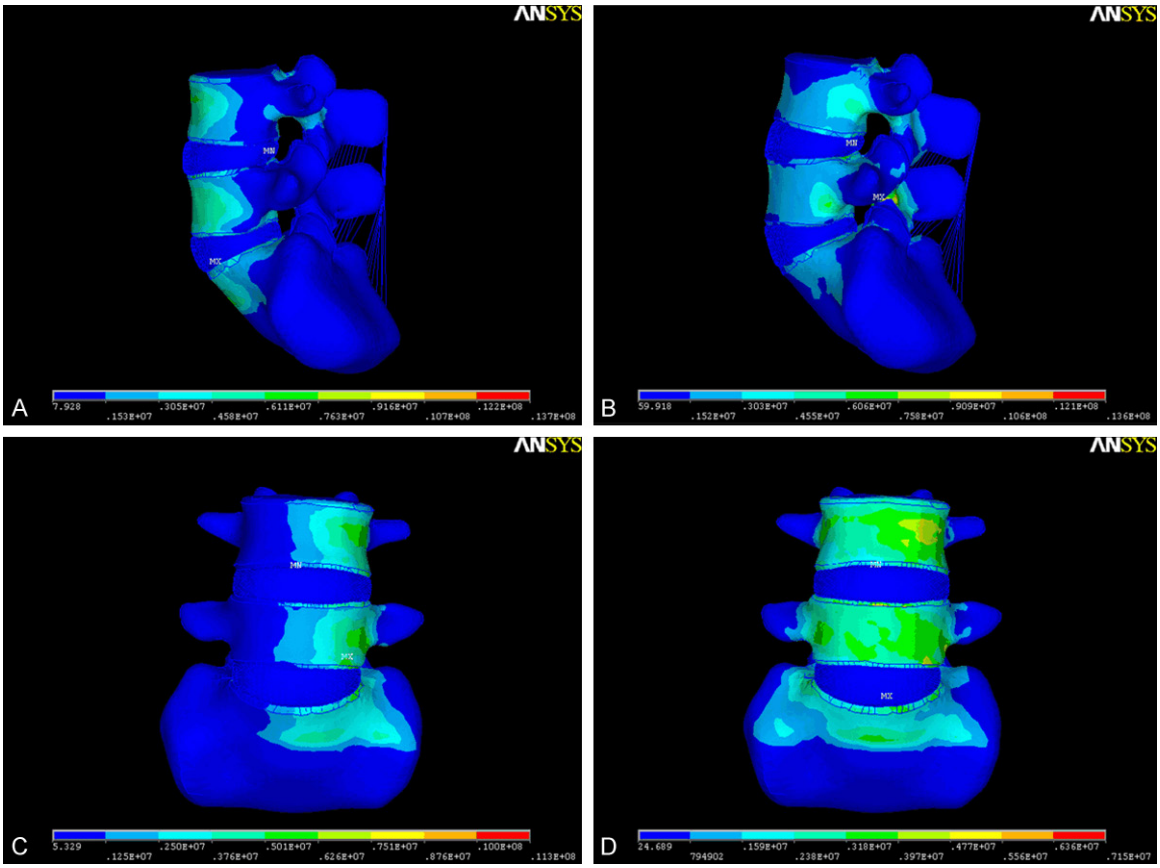

Figure 4. Von Mises stress distributions on intact lumbosacral vertebrae in (A) flexion, (B) extension, (C) lateral bending and (D) axial rotation.

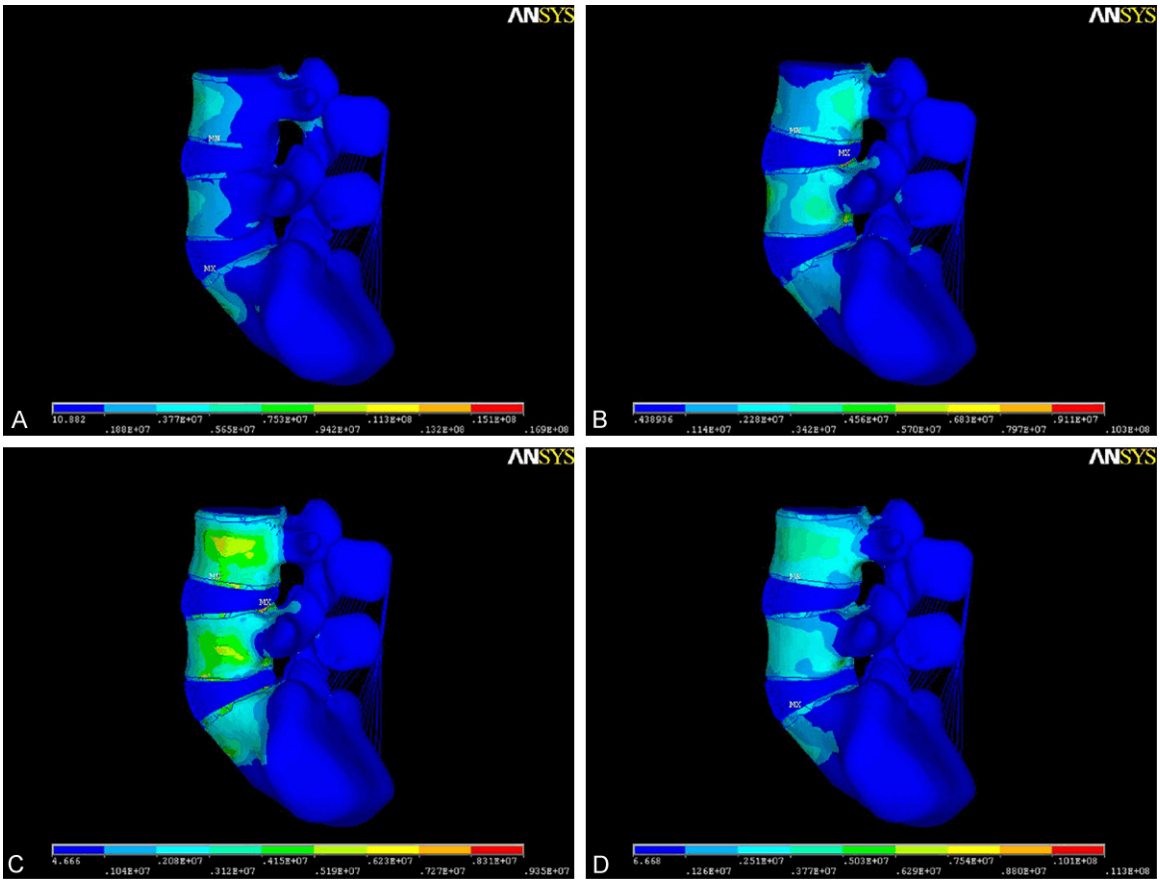

Figure 5. Von Mises stress distributions on lumbosacral vertebrae in all surgery-simulated models during (A) flexion, (B) extension, (C) lateral bending and (D) axial rotation.

previous tests in vitro shown in **Figure 3** [18-20]. It indicated that motion pattern of the present intact model ran in good agreement with that of previously published data. The surgery-simulated FE models created from the intact model were, therefore, valid for further analysis.

Stress distribution on lumbosacral vertebrae

In the intact model, a relatively high stress was generated mainly in the anterior portion of the vertebral body during flexion. During extension, it was generated in the posterior element of the intact model. When lateral bending was exercised, the Von Mises stress was distributed to unilateral portion of the vertebral body while it located over the vertebral body, especially on the facet joints under axial rotation (**Figure 4**). Illustrated in **Figure 5** was the stress distribution on lumbosacral vertebrae of surgery-simulated models. During rigid fixation with the transsacral rod, a higher stress was concentrating at the bone-rod interface under all loading conditions. It demonstrated that the maximal stress was locating over the anterior and anterolateral region of S1 vertebra when flexion and axial rotation were exercised respectively, while such stress concentration moved to the posterior and lateral region of L5 vertebra during extension and lateral bending respectively. It suggested that the highest stress value came to be 17.1MPa in the spondylolysis model during flexion and the maximal stress values were close under all conditions among the surgery-simulated models (**Table 2**; **Figure 6**).

Stress distribution on axial transsacral rod

A high stress concentrated on the middle part of the axial transsacral rod and the maximal stress were localizing at the first or second thread pitches above or below the middle part under flexion, extension, lateral bending and axial rotation (**Figure 7**). Stress distribution on the rod as shown in **Figure 8** indicated a gradu-

Table 2. The maximal Von Mises stress concentrated on lumbosacral vertebrae and axial transsacral rod (MPa)

Group	Flexion		Extension		Lateral Bending		Axial Rotation	
	vertebrae	rod	vertebrae	rod	vertebrae	rod	vertebrae	rod
AL	16.9	92	9.98	119	9.4	131	11.2	119
AL+SP	17.1	90	10.5	117	9.35	131	11.3	124
AL+HF	16.9	92	10.3	117	9.35	131	11.3	124
AL+FA	16.9	92	9.96	119	9.35	131	11.2	119

AL: standalone AxiaLIF model, AL+SP: spondylolysis model with standalone AxiaLIF procedure, AL+HF: left hemifacetectomy model with standalone AxiaLIF procedure, AL+FA: left facetectomy model with standalone AxiaLIF procedure.

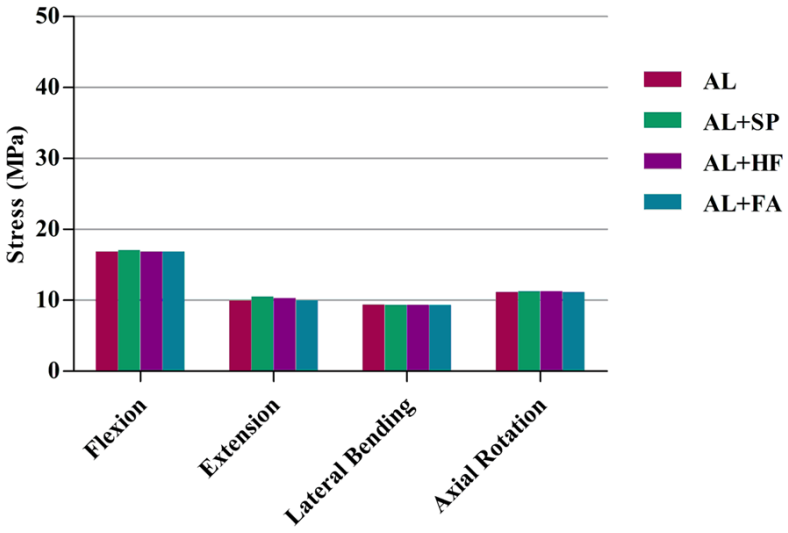

Figure 6. Comparisons of maximum Von Mises stresses on lumbosacral vertebrae among all models in flexion, extension, lateral bending and axial rotation. AL: standalone AxiaLIF model, AL+SP: spondylolysis model with standalone AxiaLIF procedure, AL+HF: left hemifacetectomy model with standalone AxiaLIF procedure, AL+FA: left facetectomy model with standalone AxiaLIF procedure.

al stress reduction from the middle part toward both ends. The highest stress value turned out to be 131 MPa as recorded in lateral bending (**Table 2**). The differences of maximal stress among the four surgery models were not significant illustrated in **Figure 9**.

Discussion

Since biomechanical test of AxiaLIF mainly focuses on the effects on external moment-rotation, FEA, supplementary to biomechanical test, can help to have direct analysis into the internal load sharing and stress distribution [10]. Bone remodeling and resorption may be activated if the load transfer is altered [17]. Owing to it, spinal components withstanding the stress concentration may lead to functional adaptation [17]. Nevertheless, such structural changes as stress fracture or degenerative changes are likely to take place when mechanism of osteanaphysis is disturbed in the long term [10, 17]. It can also be assumed that more stress on internal fixation devices will result in higher probability of device failure or even fracture [14]. As a result, the present study concentrates on postoperative evaluation of the modified stress distribution on lumbosacral vertebrae and axial transsacral rod by FEA.

This study illustrated that a transsacral rod insertion obviously exerted due modification to the overall load transfer and stress distribution among the spinal components under all conditions. The rod unloaded most of the stress on the vertebral body, especially the stress generated on posterior column of the vertebral body during extension, lateral bending and rotation, in addition to stepping up the stability of lumbosacral vertebrae. A high concentration of stress could be detected at the bone-rod interface under all loading conditions. The highest stress generated over the vertebral body had not exceeded the yield strength of cortical bone and cancellous bone. It signals the little possibility of stress fracture or degenerative changes in the long term [24-26], which can be concluded that the mechanical system is likely to be stable after the AxiaLIF procedure. As mentioned by previous FEA report of AxiaLIF, the novel lumbosacral fusion system allows good stabilization of the segment [27]. Coincidentally, the incidence of such complications as pseudarthrosis, migration, subsidence, disc degeneration or bone fracture has been reported rarely and a favorable fusion rate has been consid-

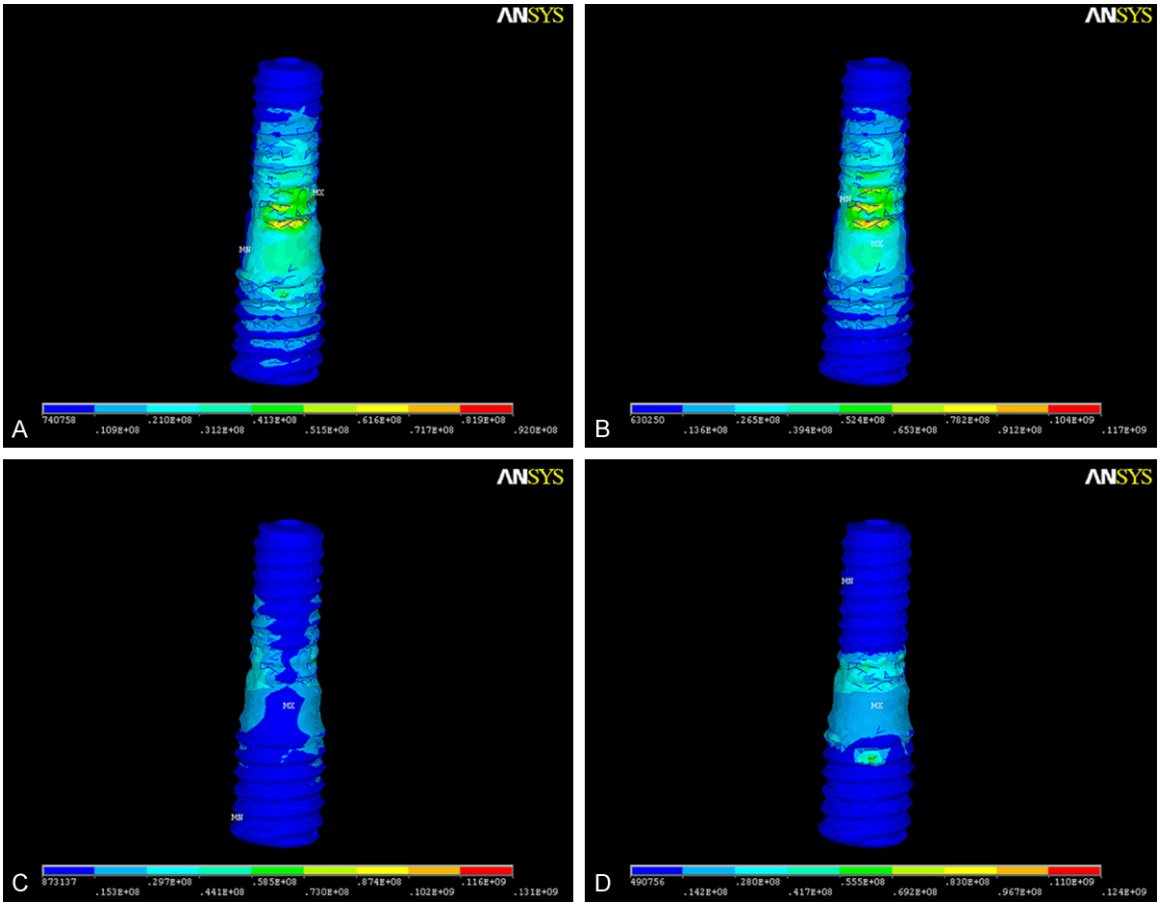

Figure 7. Von Mises stress distributions on axial transsacral rod in all surgery-simulated models during (A) flexion, (B) extension, (C) lateral bending and (D) axial rotation.

ered when patients undergo interbody fusion with the transsacral rod by a number of clinical researches [5, 7, 28].

Indicated in the previous FEA research by Xu [29], the relatively high stress concentrated at the point of interbody fusion and middle part of the rod, while all the highest values being localized to the upper and lower threads closest to the middle part. Similarly in this study, a record of 131 MPa stood as the highest stress value that was endured by axial transsacral rod in all the surgery-simulated models. It happened when lateral bending was exercised. Rod breakage may ensue from an overload that exceeds 850-900 MPa, the yield stress of titanium alloy [30]. As a result, the standalone axial transsacral rods in surgery-simulated models have been designed of ample stress resistance to meet the basic requirements of the body's normal activities. The highest stress level concentrated at one or two thread pitches below or above the middle part of the axial transsacral rod with a gradual stress reduction from the middle part towards both ends under all circumstances. It demonstrates the necessity for axial transsacral rod to have full contact with the inferior edge of L5 vertebra and superior edge of S1 vertebra in an attempt to achieve harvest bone fusion at L5-S1 intervertebral space and provide construct stability.

There were no obvious differences displayed in the present study between the spondylolysis model, unilateral facet deficit model and standalone AxiaLIF model when comparison was made to assess the maximal stress imposed on lumbosacral vertebrae or axial transsacral rod. Considering the spondylolysis model, the load bearing was primarily attributed to anterior columns of lumbosacral vertebrae after standalone AxiaLIF procedure, with pars defect in the region of posterior bony components. Since the vertebra-rod-vertebra system turned

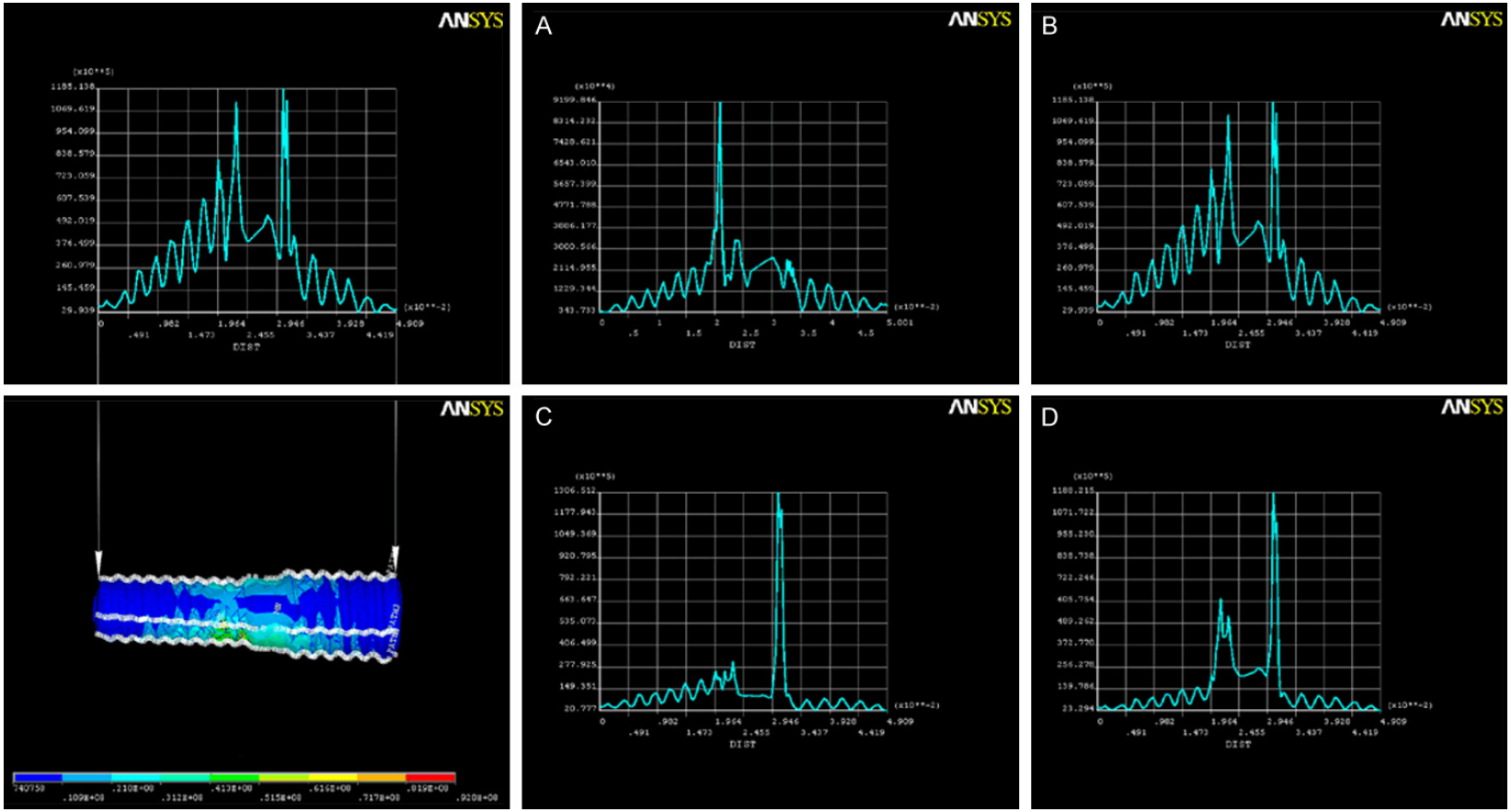

Figure 8. Line chart describing tendency of stress distributions on axial transsacral rod in all surgery-simulated models during (A) flexion, (B) extension, (C) lateral bending and (D) axial rotation.

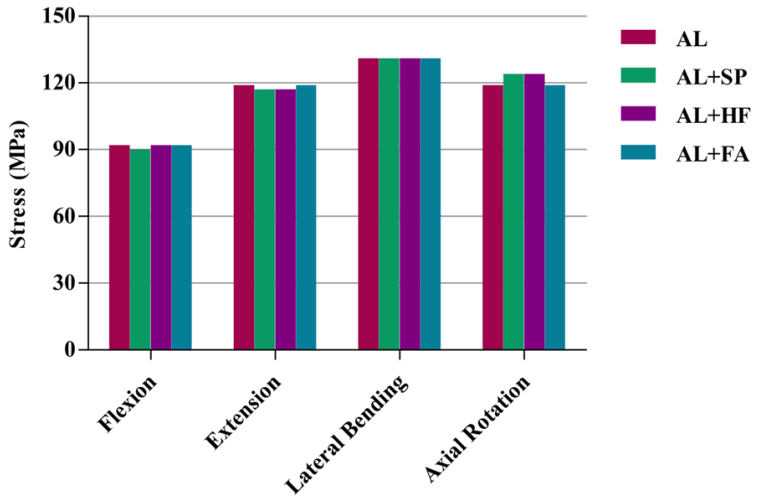

Figure 9. Comparisons of maximum Von Mises stresses on axial transsacral rod among surgery-simulated models in flexion, extension, lateral bending and axial rotation. AL: standalone AxiaLIF model, AL+SP: spondylolysis model with standalone AxiaLIF procedure, AL+HF: left hemifacetectomy model with standalone AxiaLIF procedure, AL+FA: left facetectomy model with standalone AxiaLIF procedure.

into a primary load-bearing unit, functional adaptation of spinal components resulting from remarkable stress concentration was not likely to occur. Therefore, standalone AxiaLIF can be carried out for patients with lumbosacral instability, and spondylolysis seems to be a favorable indication for AxiaLIF technique.

As mentioned above, the maximal Von Mises stress concentrated on the unilateral facet deficit model was neither beyond the yield strength of vertebra nor rod that made of titanium alloy. Compared to the standalone AxiaLIF model, an ideal biomechanical result for standalone AxiaLIF procedure in patients with unilateral facet deficit is in support of the supposition that direct unilateral decompression exerts only a minor influence on load transfer. Such patients who suffered from lumbosacral degenerative diseases showing symptoms of spinal stenosis, can benefit from unilateral decompression by MEDL in combination with AxiaLIF. The incidence of iatrogenic lumbosacral instability is likely to be very low.

Although all the FE models in this study were built with reference to the actual anatomic structures and material properties, it is apparent that a few confounding factors and limitations do exist. Although the behaviors of trunk muscles and primary ligaments were simulated by the boundary and loading conditions that has been extensively used in related tests, the complicated external load conditions in vivo such as the real situations of muscle contraction and ligaments tension were not investigated. Nevertheless, average intersegmental motion in the present intact model was similar to it recorded in previous studies, which demonstrated a satisfactory result for validation of FE model. Another confounding factor is that AxiaLIF is actually carried out among the patients with lumbosacral degenerative diseases. However, the material properties of various components in the degenerative model were not simulated, which might induce alteration in stress distribution and, in the final analysis, result in uncertain effects. Despite this, biomechanical comparisons of various internal fixation system have been evaluated successfully in numerous published FEA literatures through the application of normal spinal geometry to simplify the models. Furthermore, the present surgery-simulated models were designed without considering bone fusion at L5-S1 intervertebral space in an attempt to immediately evaluate the stress distribution after operation; the axial transsacral rod was assumed to be fixed with bones and not to allow any motion. Since bone fusion is extremely important for structural stabilization contributing to share local stress of rod, such effects of stress distribution will be explained in the future study. In addition, generic conclusions were based upon the geometrical model of a specific healthy volunteer in the Asian populations, the influences of inter-individual variations and racial differences were not excluded. Due to the limitations of this study, the conclusions cannot be directly incorporated in individual patient's evaluation. Considering that FE models cannot reproduce the accurate results of cadaveric specimens study or copy the exact surgical procedures, further biomechanical studies of large sample are called forth to determine the intersegmental motion of all surgery-simulated models with due consideration

of bone fusion and muscle force involved. The effects on stability of all surgery-simulated models should be estimated postoperatively during different stages in future studies.

In conclusion, the present study demonstrated that rigid fixation unloads most of the stress on the vertebral body during all loading conditions when the insertion of axial transsacral rod has been performed. The standalone AxiaLIF offers sufficient stress resistance, thus meets the basic requirements for normal activities of patients. In comparison with other surgery-simulated models, only insignificant influence is exerted on load transfer in patients with spondylolysis or unilateral facet deficit. Considerable alteration in stress distribution seems not to be evoked in patients suffering from spondylolysis after AxiaLIF procedure, or such patients demanding unilateral direct decompression by MEDL in combination with AxiaLIF.

Acknowledgements

We acknowledge the work of Dr. Liangming Zhang, Dr. Bin Liu, and Dr. Jianwen Dong from Department of Spine Surgery, Third Affiliated Hospital, Sun Yat-sen, for their help in conducting this study and overseeing the project.

Disclosure of conflict of interest

None.

Address correspondence to: Dr. Limin Rong, Department of Spine Surgery, Third Affiliated Hospital, Sun Yat-sen University, No. 600 Tianhe Road, Tianhe District, Guangzhou 510630, China. E-mail: ronglm21@163.com

References

[1] Cragg A, Carl A, Casteneda F, Dickman C, Guterman L and Oliveira C. New percutaneous access method for minimally invasive anterior lumbosacral surgery. J Spinal Disord Tech 2004; 17: 21-28.

[2] Marotta N, Cosar M, Pimenta L and Khoo LT. A novel minimally invasive presacral approach and instrumentation technique for anterior L5-S1 intervertebral discectomy and fusion: technical description and case presentations. Neurosurg Focus 2006; 20: E9.

[3] Akesen B, Wu C, Mehbod AA and Transfeldt EE. Biomechanical evaluation of paracoccygeal transsacral fixation. J Spinal Disord Tech 2008; 21: 39-44.

[4] Ledet EH, Tymeson MP, Salerno S, Carl AL and Cragg A. Biomechanical evaluation of a novel lumbosacral axial fixation device. J Biomech Eng 2005; 127: 929-933.

[5] Tobler WD, Gerszten PC, Bradley WD, Raley TJ, Nasca RJ and Block JE. Minimally invasive axial presacral L5-S1 interbody fusion: two-year clinical and radiographic outcomes. Spine (Phila Pa 1976) 2011; 36: E1296-1301.

[6] Aryan HE, Newman CB, Gold JJ, Acosta FL Jr, Coover C and Ames CP. Percutaneous axial lumbar interbody fusion (AxiaLIF) of the L5-S1 segment: initial clinical and radiographic experience. Minim Invasive Neurosurg 2008; 51: 225-230.

[7] Tobler WD and Ferrara LA. The presacral retroperitoneal approach for axial lumbar interbody fusion: a prospective study of clinical outcomes, complications and fusion rates at a follow-up of two years in 26 patients. J Bone Joint Surg Br 2011; 93: 955-960.

[8] Bohinski RJ, Jain VV and Tobler WD. Presacral retroperitoneal approach to axial lumbar interbody fusion: a new, minimally invasive technique at L5-S1: Clinical outcomes, complications, and fusion rates in 50 patients at 1-year follow-up. SAS J 2010; 4: 54-62.

[9] Khoo LT and Fessler RG. Microendoscopic decompressive laminotomy for the treatment of lumbar stenosis. Neurosurgery 2002; 51: S146-154.

[10] Guan Y, Yoganandan N, Maiman DJ and Pintar FA. Internal and external responses of anterior lumbar/lumbosacral fusion: nonlinear finite element analysis. J Spinal Disord Tech 2008; 21: 299-304.

[11] Kim Y and Kim TW. Finite Element Analysis of the Effects of Pedicle Screw Fixation Nut Loosening on Lumbar Interbody Fusion Based on the Elasto-Plateau Plasticity of Bone Characteristics. Spine (Phila Pa 1976) 2010; 599-606.

[12] Rohlmann A, Burra NK, Zander T and Bergmann G. Comparison of the effects of bilateral posterior dynamic and rigid fixation devices on the loads in the lumbar spine: a finite element analysis. Eur Spine J 2007; 16: 1223-1231.

[13] Pitzen T, Geisler FH, Matthis D, Muller-Storz H, Pedersen K and Steudel WI. The influence of cancellous bone density on load sharing in human lumbar spine: a comparison between an intact and a surgically altered motion segment. Eur Spine J 2001; 10: 23-29.

[14] Duan Y, Zhang H, Min SX, Zhang L and Jin AM. Posterior cervical fixation following laminectomy: a stress analysis of three techniques. Eur Spine J 2011; 20: 1552-1559.

[15] Pintar FA, Yoganandan N, Myers T, Elhagediab A and Sances A Jr. Biomechanical properties

of human lumbar spine ligaments. J Biomech 1992; 25: 1351-1356.
[16] Sharma M, Langrana NA and Rodriguez J. Role of ligaments and facets in lumbar spinal stability. Spine (Phila Pa 1976) 1995; 20: 887-900.
[17] Polikeit A, Ferguson SJ, Nolte LP and Orr TE. Factors influencing stresses in the lumbar spine after the insertion of intervertebral cages: finite element analysis. Eur Spine J 2003; 12: 413-420.
[18] Yamamoto I, Panjabi MM, Crisco T and Oxland T. Three-dimensional movements of the whole lumbar spine and lumbosacral joint. Spine (Phila Pa 1976) 1989; 14: 1256-1260.
[19] Panjabi MM, Oxland TR, Yamamoto I and Crisco JJ. Mechanical behavior of the human lumbar and lumbosacral spine as shown by three-dimensional load-displacement curves. J Bone Joint Surg Am 1994; 76: 413-424.
[20] Erkan S, Wu C, Mehbod AA, Hsu B, Pahl DW and Transfeldt EE. Biomechanical evaluation of a new AxiaLIF technique for two-level lumbar fusion. Eur Spine J 2009; 18: 807-814.
[21] Zheng L, Li Z, Li Q, Ji F and Cai Z. Finite element analysis of lumbosacral reconstruction after partial sacrectomy. Med Sci Monit 2014; 20: 889-893.
[22] Natarajan RN, Garretson RB 3rd, Biyani A, Lim TH, Andersson GB and An HS. Effects of slip severity and loading directions on the stability of isthmic spondylolisthesis: a finite element model study. Spine (Phila Pa 1976) 2003; 28: 1103-1112.
[23] Bresnahan L, Ogden AT, Natarajan RN and Fessler RG. A biomechanical evaluation of graded posterior element removal for treatment of lumbar stenosis: comparison of a minimally invasive approach with two standard laminectomy techniques. Spine (Phila Pa 1976) 2009; 34: 17-23.
[24] Natali AN and Meroi EA. A review of the biomechanical properties of bone as a material. J Biomed Eng 1989; 11: 266-276.
[25] Reilly DT and Burstein AH. Review article. The mechanical properties of cortical bone. J Bone Joint Surg Am 1974; 56: 1001-1022.
[26] Morgan EF and Keaveny TM. Dependence of yield strain of human trabecular bone on anatomic site. J Biomech 2001; 34: 569-577.
[27] Boustani HN, Rohlmann A, Abouezzeddine O, Bergmann G and Zander T. Stiffening effect of a transsacral fusion system for the lumbosacral junction. A probabilistic finite element analysis and sensitivity study. Orthopade 2011; 40: 162-168.
[28] Gundanna MI, Miller LE and Block JE. Complications with axial presacral lumbar interbody fusion: A 5-year postmarketing surveillance experience. SAS J 2011; 5: 90-94.
[29] Xu HG, Yang XM, Wu TL, Wang H, Chen XW, Wang LT, Jin S and Liu P. Finite element analysis of the screw in percutaneous axial lumbosacral interbody fusion. Orthop Surg 2010; 2: 207-210.
[30] Long M and Rack HJ. Titanium alloys in total joint replacement–a materials science perspective. Biomaterials 1998; 19: 1621-1639.